(Received 12 June 2025, Accepted 3 August 2025, Scheduled 20 August 2025)

Snail-Like Golden Spiral Triboelectric Nanogenerator for All-Directional Wave Energy Harvesting

Yuxuan Tong[1], Xin Zhou[1,*], Xiaobing Niu[1], and Xinhua Ye[2]

[1] *Department of Ship Electrical Engineering College, Dalian Maritime University, Dalian, China*
[2] *Department of Electrical and Information Engineering, Hunan University, Dalian, China*

ABSTRACT: In recent years, harvesting abundant, clean, and renewable wave energy from the ocean has become one of the most promising ways to obtain electricity. However, the multi-directional nature of waves and the low frequency of the movement pose a current challenge. We designed and fabricated an all-directional triboelectric nanogenerator (AD-TENG) with a biomimetic snail golden spiral. It consists of an electric energy collector in the vertical direction and another in the horizontal direction, and mainly operates through the contact separation method. The AD-TENG converted mechanical energy into electrical energy with the swinging of the pendulum and folding movements. The spiral structure of AD-TENG can harvest energy in all horizontal directions, and the wiring is simple, requiring only two positive and negative wires. In a water wave environment, the AD-TENG charged a capacitor of 100 μF to a voltage of 3 V in 2 minutes, lighting up 150 LED bulbs. The experiment measured the peak-to-peak voltage (Vpp) from 15 different angles and calculated the error "e" as 4.6%. The multi-degree-of-freedom energy harvesting and adaptability to various water wave motions of the AD-TENG offer great potential for the development of self-powered marine sensors.

1. INTRODUCTION

Over the past few decades, wind energy and solar energy have been two important and rapidly developing clean energy sources. However, solar cell materials cause significant environmental pollution, and both night and cloudy days can affect the harvesting and utilization of solar energy. In addition, the noise generated by wind turbines also has an impact on the ecological environment and can only operate in specific windy areas [1–4]. 71% of the Earth's ocean resources have resulted in abundant reserves of wave energy, rich energy distribution, and zero carbon emissions [5]. However, traditional electromagnetic generators (EMGs) face many challenges in sea wave energy exploration in terms of insufficient low-frequency wave conversion efficiency [6], large volume, and heavy equipment.

Triboelectric nanogenerator (TENG) combines friction charging with electrostatic induction and uses displacement current as the driving force, effectively converting various forms of mechanical energy into electrical energy [7–13]. TENG can effectively harvest water wave energy using various low-cost materials such as fluorinated ethylene propylene (FEP), ethylene-vinyl acetate (EVA), and copper. It has the advantages of simple structure, high low-frequency conversion efficiency, and ease of floating on the water surface. TENG is considered an effective method for harvesting blue energy [14–18].

From Table 1 (see Supporting Information), it can be seen that the negative electrode friction material, FEP, has high electron affinity and is suitable for the use as a flexible material, which is in line with the surface design of this work. Additionally, its good flexibility makes it suitable for reciprocating stretching movements. The positive electrode friction materials, copper and Al, have very low electron affinity, but Al is more active and not suitable for welding. In addition, copper has outstanding ductility and is suitable for the use as a surface material. Besides, EVA is suitable for flexible devices and has a low cost, and polyethylene terephthalate (PET) has certain hardness and strength, making it suitable for vertical-directional elastic materials [19–21].

Lin et al. developed a TENG inspired by a pendulum (P-TENG), where the pendulum swings back and forth once within a motion cycle, equivalent to two contact-separation movements, doubling its output frequency and effectively utilizing water and wind energy [22]. Once an external force triggers P-TENG, the friction layer of the pendulum will swing back and forth relative to each other and periodically come into contact with the slightly striped thin polytetrafluoroethylene (PTFE). Although P-TENG can increase the output frequency and effectively harvest wave energy, it does not fully utilize the internal space of the pendulum swing, resulting in a low output efficiency. Ding et al. proposed a multilayered TENG (M-TENG) spring model based on a folded structure. By having the pendulum moved back and forth and collided with the contact layer, the folded part is contacted to harvest multi-directional wave energy using the magnetic-field-assisted TENG (MFA-TENG) method [23]. Although the internal space utilization of the pendulum has been improved, it can only harvest energy from six specific angles and cannot achieve full-directional energy harvesting. Wen et al. designed and fabricated a TENG with a biomimetic flower-shaped structure, which can harvest kinetic energy in six degrees of freedom. The petal part of the TENG

* Corresponding author: Xin Zhou (Xinchow@dlmu.edu.cn).

harvests the kinetic energy of translational motion in the horizontal direction, while the core TENG harvests the kinetic energy of vertical motion [24]. The biomimetic flower-shaped TENG cannot harvest kinetic energy in higher degrees of freedom. Compared to the pendulum motion, the periodic motion frequency of the folded TENG is lower.

We proposed a biomimetic snail shell structure, which is an efficient piezoelectric energy collector. The AD-TENG consists of a horizontal gold spiral structure piezoelectric energy collector and a vertical folded piezoelectric energy collector. It can collect energy from all directions (including 360° in the horizontal direction and vertically). Based on the structural characteristics of the golden spiral line, AD-TENG can fully utilize the spatial density and maximize the output performance [25, 26]. The backplate of the horizontal TENG is made of soft EVA material, which can increase the contact area and soft contact in the bending structure, thereby improving the contact efficiency between the friction layers. AD-TENG collects mechanical energy through the oscillatory motion resulting from its simple structure, the ability to achieve multi-frequency output, and superior performance [27, 28]. By studying the influence of the number of spiral layers and weight on the output energy of the horizontal TENG, a significant improvement in output energy was achieved. Additionally, the performance of AD-TENG under different inclination angles was also investigated. By changing the inclination angle, it was demonstrated that AD-TENG has the ability to collect energy from multiple directions of wave energy. Finally, we successfully demonstrated the practical application value of AD-TENG by illuminating LEDs and providing power, and its application prospects in the marine field.

As can be seen from Table 2 (see Supporting Information), our work demonstrates significant advantages in the following aspects: The ability to harvest energy simultaneously in both horizontal and vertical directions; a near-zero horizontal omnidirectional angular resolution, which enables 360° energy collection on the horizontal plane; low cost without complex manufacturing processes; and a reduced number of electrodes. While the power density of the AD-TENG is 1.2 W/m^3, its output performance is relatively average, which indicates that there is still room for improvement in its power output [29–32].

2. RESULT

2.1. Structural Designs and Fabrications

All directional TENG (AD-TENG) consists of a horizontally 360° swinging bouncing chamber and a folded TENG (Fig. 1(a)). Inspired by the golden spiral of a snail shell (Fig. 1(b)), the AD-TENG includes multiple layers of snail-like rotary TENG (SR-TENG), as shown in Fig. 1(c) and two vertical folded TENGs (VF-TENGs), as illustrated in Fig. 1(d). The inner layer of the golden spiral of SR-TENG is adhered to the pendulum. The upper end of the pendulum is fixed to the upper end of the internal acrylic cylindrical barrel through an inelastic connecting rod. The structural shape of the pendulum is conical, wide at the top, narrow at the bottom, and hollow inside, which can add heavy objects. The SR-TENG is formed by rotating a single contact-separation unit structure multiple times to create a TENG with multi-layer contact-separation functions. Its base is a 1 mm thick, 12 cm wide EVA foam board, with a copper foil electrode (50 μm) attached to one side of the EVA and the other side composed of a copper foil electrode (50 μm) and FEP with a thickness of 50 μm bonded together. The assembled SR-TENG is separately encapsulated in an acrylic cylindrical container with a diameter of 11 cm, a height of 20 cm, and a thickness of 1 mm. The substrate of VF-TENG adopts polyethylene terephthalate (PET). Each VF-TENG has 7 folding units, and each folding unit is composed of two copper foil electrodes (50 μm), each 6 cm long and 4 cm wide, with FEP film (50 μm) covering one side. Then, the SR-TENG is vertically installed above the VF-TENG, with the VF-TENG located at the bottom of the container. AD-TENG and VF-TENG are sealed together in an acrylic cylindrical barrel with a diameter of 14 cm and a height of 30 cm.

It can be known from Fig. 1(e) that the internal contact separation unit layer of SR-TENG is similar to the golden spiral structure of a snail shell, enabling SR-TENG to harvest wave energy in the horizontal 360° direction. Meanwhile, as shown in Fig. 1(f), the SR-TENG and VF-TENG are vertically fixed as a whole. It is capable of harvesting the energy in the vertical direction brought by the surging of waves. As shown in Fig. 1(g), due to the mutual combination of SR-TENG and VF-TENG, wave energy can be harvested in the 0–180° tilt direction.

2.2. Horizontal Working Mechanism and Its Output Performance

Under the action of waves, the working process of SR-TENG shows a unique mechanism, as shown in Fig. 2(a). When the water wave surges from the right side, the right part of the SR-TENG is lifted and tilted to the left, and this action drives the pendulum to swing to the left. During the swinging process of the pendulum, it successively strikes the contact and separation unit layers and eventually hits the inner wall of the container, causing the right side of SR-TENG to separate while the left side comes into contact due to pressure. Due to the helical curved surface design of the contact separation unit layer composed of copper foil and FEP, compared with the planar structure, it can significantly increase the contact separation area. The working principle of SR-TENG in waves is shown in Fig. 2(b). When the copper foil is in full contact with FEP and rubbed against it, the charges of the two materials reach a saturated state 2(b)(I). At this point, the surface of FEP becomes negatively charged due to friction, while the copper foil becomes positively charged. When water waves flow from the left side, the left side of the SR-TENG is lifted and tilted to the right. The pendulum strikes the inner wall of the container in the opposite direction, causing the left side to separate and the right side to come into contact and compress. The periodic movement of the contact separation layer continuously repeats the process of "contact-separation". In the contact state, as shown in Fig. 2(b)(II), the negative charges on the FEP surface generate a potential difference between the two copper foil electrodes through electrostatic induction, promoting the movement of positive charges on the copper foil

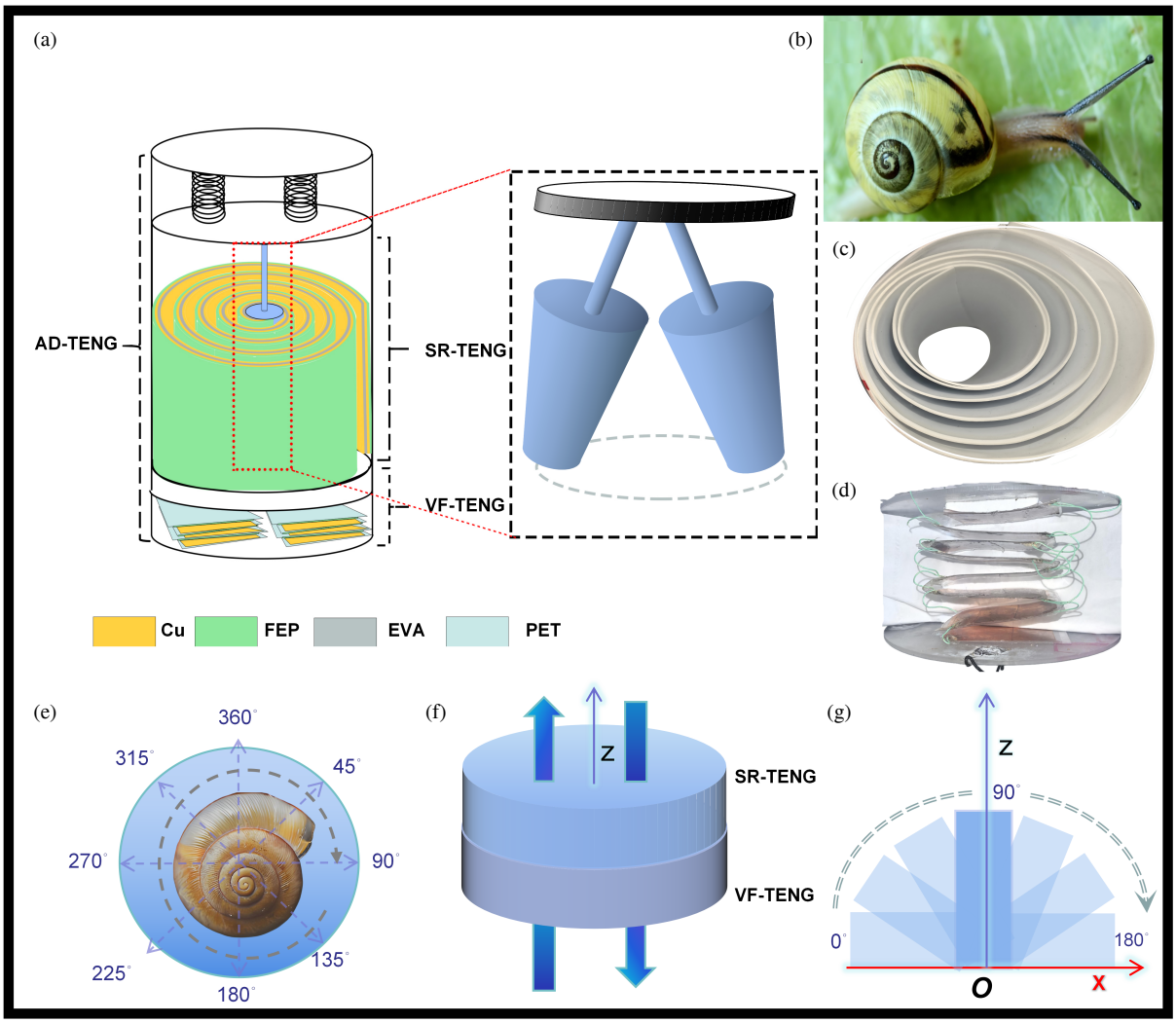

FIGURE 1. (a) AD-TENG structure schematic diagram. (b) Optical image of gold spiral from a snail shell. (c) Optical image of SR-TENG. (d) Optical image of VF-TENG. (e) Schematic diagram of 360° all-directional energy harvesting. (f) Schematic diagram of vertical energy harvesting. (g) Schematic diagram of 3D omnidirectional energy harvesting.

electrodes. In contact state 2(b)(III), the copper foil and FEP generate frictional electrification through contact. The surface of FEP is negatively charged, while the copper foil is positively charged. When the contact surface separates, as shown in Fig. 2(b)(IV), the potential difference at the contact surface gradually decreases, and the charge returns to the original electrode. Therefore, under the induction of water waves, the contact separation layer operates periodically, generating an alternating potential difference with pulse changes between the two electrodes, thereby converting the energy of water wave oscillation into electrical energy for output through mechanical energy. To further understand the mechanism of the above power generation process, COMSOL Multiphysics software based on finite-element analysis was employed to simulate the potential distributions of TENG architectures under various operational states (in Fig. S1a).

Throughout the entire process, the swing of the pendulum drives the periodic action of the contact separation layer, and the principles of frictional electrification and electrostatic induction run through it, achieving effective energy conversion. As shown to improve the output performance of SR-TENG, optimization experiments were conducted on the structural parameters of SR-TENG. Fig. 2(d) shows SR-TENGs fabricated using EVA foam board bases with 4, 5, 6, and 7 layers. The Vpp of SR-TENG was measured, as shown in Fig. 2(e). The results indicate that the peak voltage (Vp) of SR-TENG fabricated with a 6-layer EVA foam base reached the maximum value of 92. As the number of layers increased, the Vpp of SR-TENG gradually increased.

However, when the number of layers increased to 7, due to the excessive number of layers in the spiral structure, the inner and outer layers overlapped, and SR-TENG could not fully achieve contact and separation, which might have an adverse effect on its output performance. Therefore, the number of layers in different spatial sizes would change, and the output performance would initially increase with the increase in the number of layers. However, when the maximum number of overlapping layers in the spiral structure was reached, the output per-

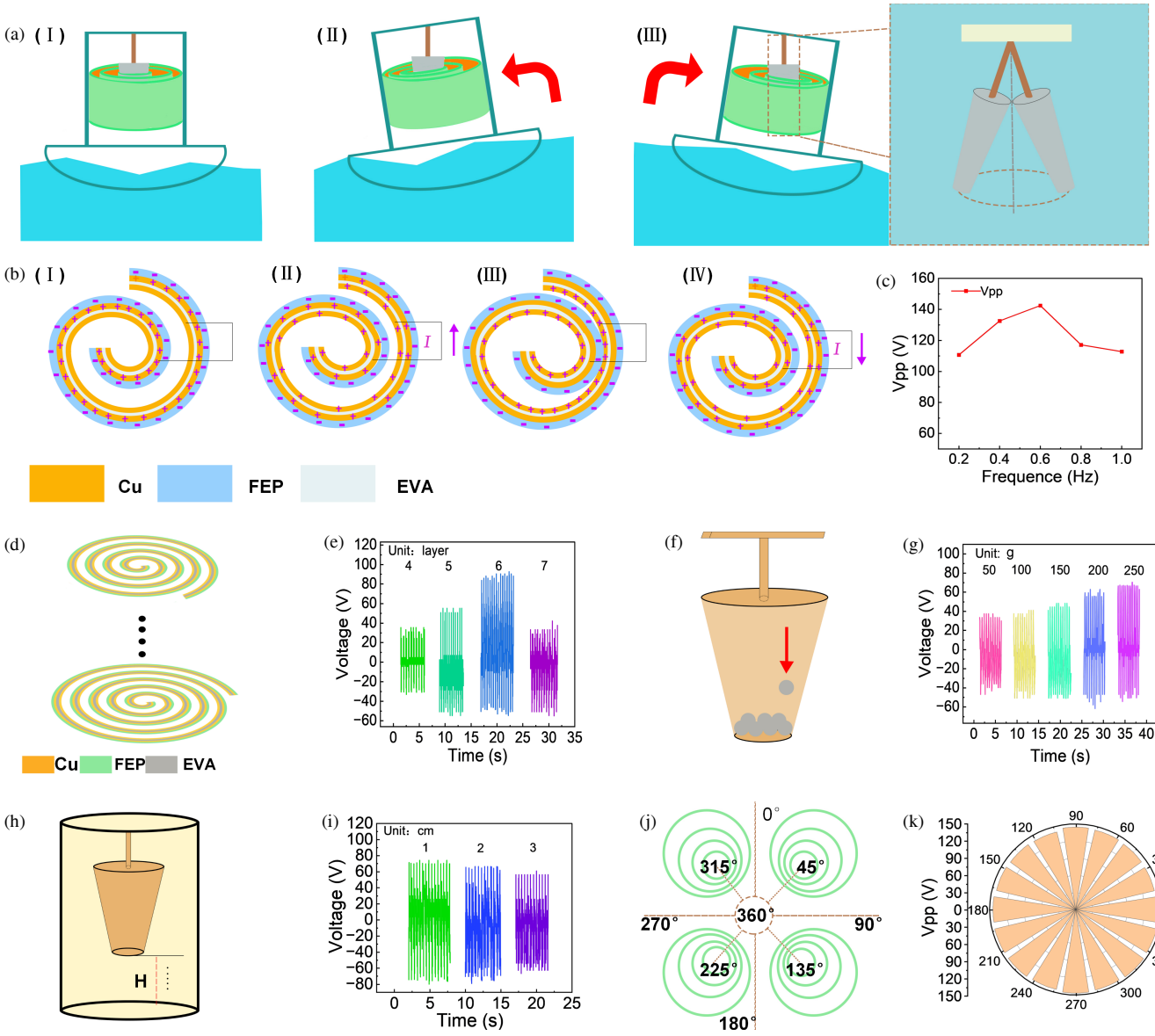

FIGURE 2. The working principle and output performance of the SR-TENG. (a) The motion process of the SR-TENG under the wave environment. (b) The working principle of the M-TENG. (c) The voltage situation of SR-TENG is under the influence of different oscillation frequencies. (d) Different layers of SR-TENGs. (e) The output voltages of SR-TENGs with different layers. (f) SR-TENGs of different weights. (g) Voltage output of SR-TENGs of different weights. (h) SR-TENGs with different pendulum heights. (i) Voltage output of SR-TENGs with different pendulum heights. (j) The 360° working process of SR-TENGs. (k) SR-TENGs provide a 360° voltage output within the working range.

formance of SR-TENG would decrease. In Fig. 2(f), weighted iron balls were added inside the pendulum to increase the pendulum's swinging inertia and the impact force on SR-TENG. At the same time, it could lower the pendulum's center of gravity, thereby enhancing the contact and separation between layers and improving the output performance.

Figure 2(g) shows the test results of the Vpp under different weights. The experimental data indicate that as the weight increased, the output performance of SR-TENG was improved to a certain extent. The experimental weight range was between 50 and 250 g. When the weight was 250 g, the Vp of SR-TENG was 72 V. Fig. 2(h) shows the comparison of experimental data at different heights of the pendulum from the bottom of the SR-TENG container. The experimental data in Fig. 2(i) indicate that as the height increased from 1 to 3 cm, the output performance of SR-TENG decreased.

Due to the increase in pendulum height, the pendulum frequency increased, and the different layers of SR-TENG could not fully achieve contact and separation. At the same time, the increase in the pendulum swing angle also prevented the pendulum from hitting the layer walls of SR-TENG to complete contact and separation. Compared to other shapes and structures, previous studies have shown that some existing container structures suffer from low space utilization, leaving the internal space underutilized. Regarding energy harvesting, certain devices are only capable of harvesting energy from uni-

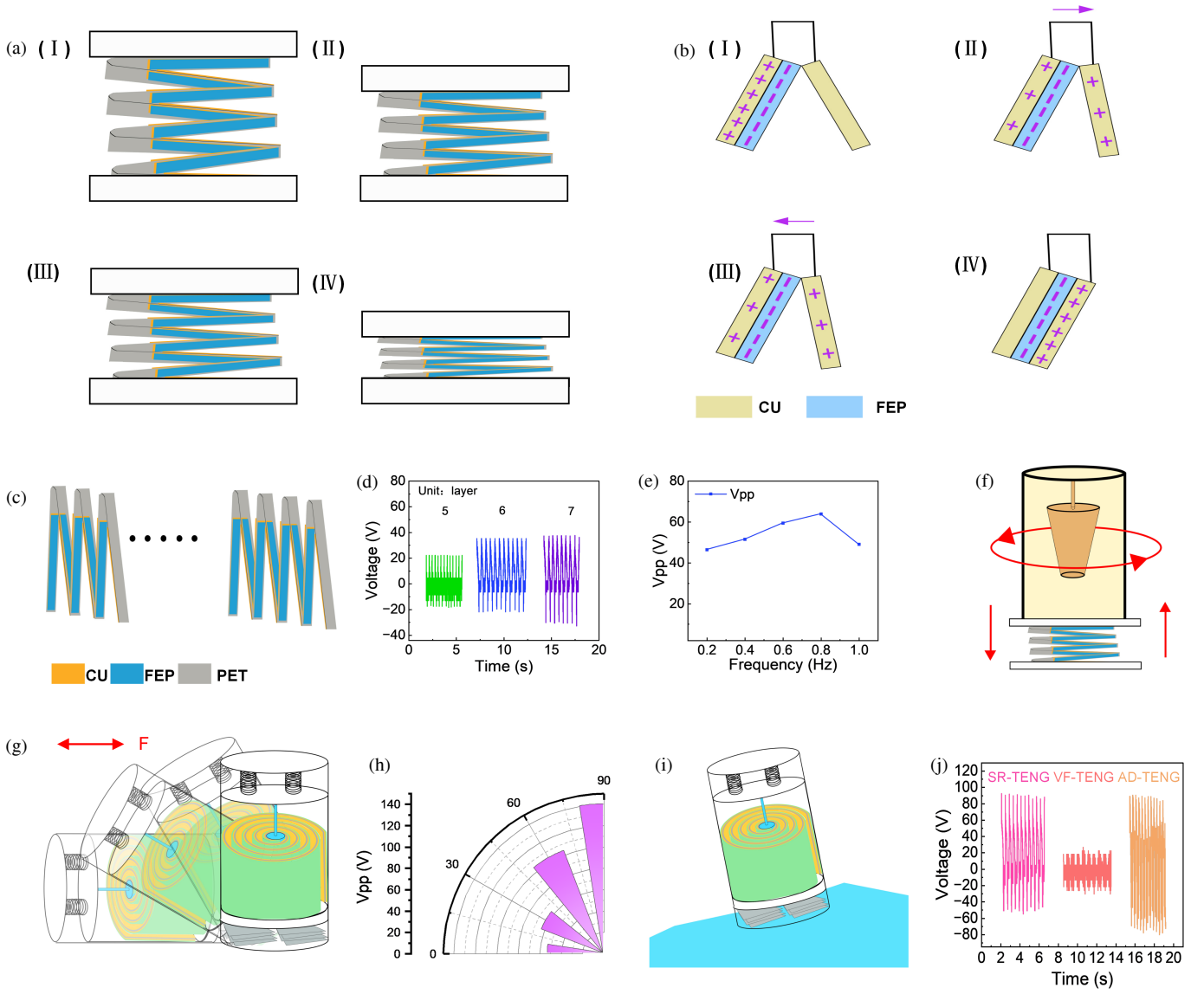

FIGURE 3. The working principle and output performance of the VF-TENG. (a) The motion process of the VF-TENG under the wave environment. (b) The working principle of the VF-TENG. (c) The voltage situation of VF-TENG is under the influence of different layers. (d) The output voltages of SR-TENGs with different layers. (e) The voltage situation of VF-TENG is under the influence of different oscillation frequencies. (f) The overall movement direction of AD-TENG. (g) AD-TENG placed at a 30° −90° angle and moving horizontally. (h) The voltage of AD-TENG is placed at an angle of 30° to 90°. (i) AD-TENG Water Wave Simulation. (j) Under the simulation of water waves, the voltage outputs of SR-TENG, VF-TENG, and AD-TENG.

directional movement. Even for devices designed for multi-directional energy harvesting, their efficiency typically peaks at specific angles and drops significantly beyond these optimal angular ranges. As shown in Fig. 2(j), this snail-like golden spiral design can achieve a similar contact and separation change process at any 360° angle in all directions. From the analysis of the mechanism mentioned above, it can be known that this structure can achieve the maximum energy harvesting efficiency at any angle in all directions. As observed from the experimental test diagram in Fig. 2(k), within a 360° rotation plane, the amplitude of Vpp of SR-TENG can be approximately regarded as a circle. And the full-direction voltage error is

$$e = \frac{V_{\max} - V_{\min}}{V_{\text{ave}}} \times 100\% \tag{1}$$

Here, e represents the offset voltage error, $V_{\max}$ the maximum voltage, $V_{\min}$ the minimum voltage, and V_{ave} the average voltage.

The experiment measured the output voltage Vpp from 15 different angles and calculated the error e as 4.6%. This verifies that SR-TENG can harvest wave energy in arbitrary directions and has outstanding stability in different output directions.

2.3. Vertical Working Mechanism and Its Output Performance

The AD-TENG is designed to harvest wave energy in a more comprehensive direction, and two groups of VF-TENGs are vertically connected to the entire bottom surface of the container and the bottom surface of the SR-TENG. The substrate

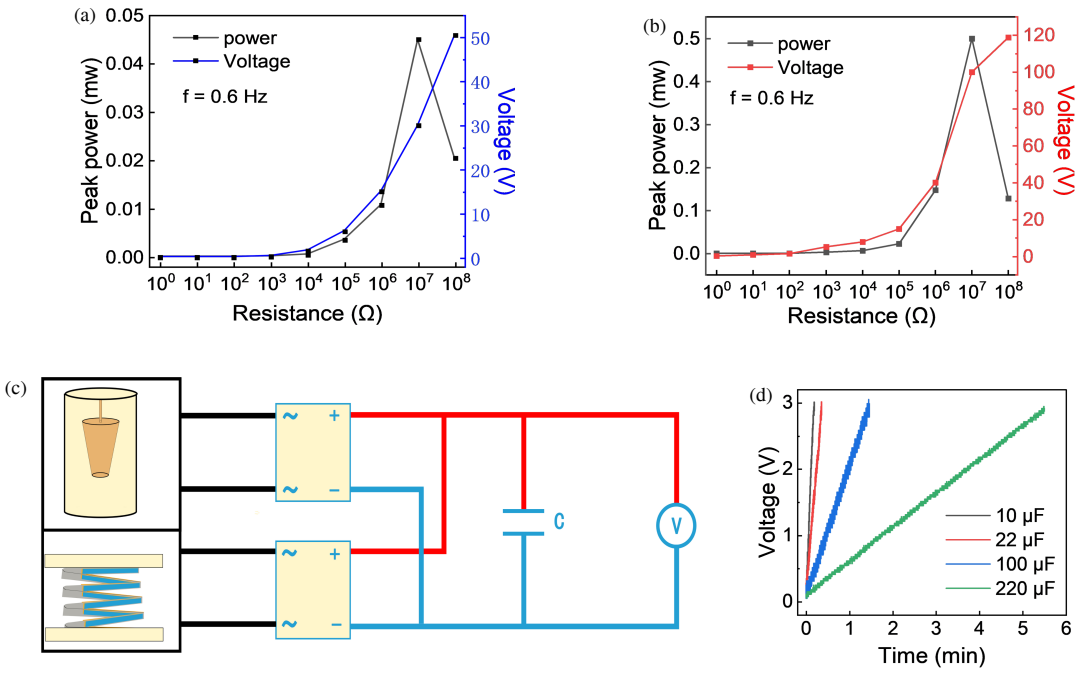

FIGURE 4. System's output performance. (a) The power output and voltage output of SR-TENG at a 0.6 Hz oscillation frequency and under different resistance loads. (b) The power output and voltage output of VF-TENG at a 0.6 Hz oscillation frequency and under different resistance loads. (c) Rectifier circuit capacitor charging diagram. (d) The charging voltage curve of different capacitors.

of the VF-TENG is made of PET material, which has high flexibility and can work like a spring.

The VF-TENG is composed of copper foil and FEP and achieves contact separation through vertical bouncing and contraction to complete the energy harvesting function. Its working principle is shown in Fig. 3(a). When being subjected to an upward vertical force in Fig. 3(a)(I), the VF-TENG continuously bounces the AD-TENG. At this time, the copper foil and FEP film fully contact and separate, and the electrons of the inner electrode transfer to the FEP film, reaching a saturated charging state in Fig. 3(b)(I). When the external force disappears in Fig. 3(a)(II)(III), the VF-TENG is pulled down and contracted under the gravitational force of the SR-TENG. During this process, the negative charges on the FEP surface cause a potential difference change between the two copper foil electrodes through electrostatic induction, prompting the positive charges on the copper foil electrodes to move in Fig. 3(b)(II)(III). At the same time, the copper foil and FEP generate triboelectricity due to contact, with the FEP surface carrying a negative charge and the copper foil carrying a positive charge. Through this vertical bouncing and contracting motion, the VF-TENG achieves the effect of contact and separation, thus effectively harvesting wave energy in the vertical direction. Finally, in the separated state in Fig. 3(a)(IV) and 3(b)(IV), as the potential difference between the two copper foil electrodes gradually decreases, the charges return to their original electrodes. Additionally, due to the induction of water wave motion, the contact-separation layer of the VF-TENG will periodically contact and separate, thereby generating pulsed alternating potential changes. The simulation results show excellent agreement with the aforementioned working mechanism, providing theoretical validation of the energy harvesting process (in Fig. S1b).

To improve the output performance of the VF-TENG, optimization experiments were conducted on its structural parameters. Fig. 3(c) shows VF-TENGs made with PET bases of 5, 6, and 7 layers. The Vpp of the VF-TENG was measured, as shown in Fig. 3(d). It can be seen from the image that the VF-TENG made with a 7-layer PET base has the maximum peak voltage Vp of 37 V. As the number of layers of the VF-TENG increases, its output performance also increases. Fig. 3(e) illustrates that the output voltage of VF-TENG varies with the frequency adjustment. As the frequency increases, it leads to a shorter oscillation period of the contact separation of the folded layers and an increased oscillation speed. Therefore, the contact ability of VF-TENG is enhanced. However, when the frequency becomes larger, the response speed of the folded layers may not keep up with the rapid changes in frequency, thereby affecting the movement of VF-TENG and, subsequently, the output voltage. At a frequency of 0.8 Hz, VF-TENG can achieve a Vpp of 67 V.

2.4. System's Output Performance

As shown in Fig. 3(f), the overall structural schematic diagram clearly shows the structural layout of SR-TENG and VF-TENG and the different directional divisions of work, as shown in Fig. 3(g). In this experiment, AD-TENG was placed at different angles of 0°, 30°, 60°, and 90°, with an interval of 30°, and tilted at the same time while applying a lateral horizontal force. In the experimental test data of Fig. 3(h), it can be seen that the superimposed output performance of SR-TENG and VF-TENG changes within the range of 0° to 90°. Since at 0° it is approximately only VF-TENG working, and at 90° it is approximately only SR-TENG working, the measured Vpp varies between 52

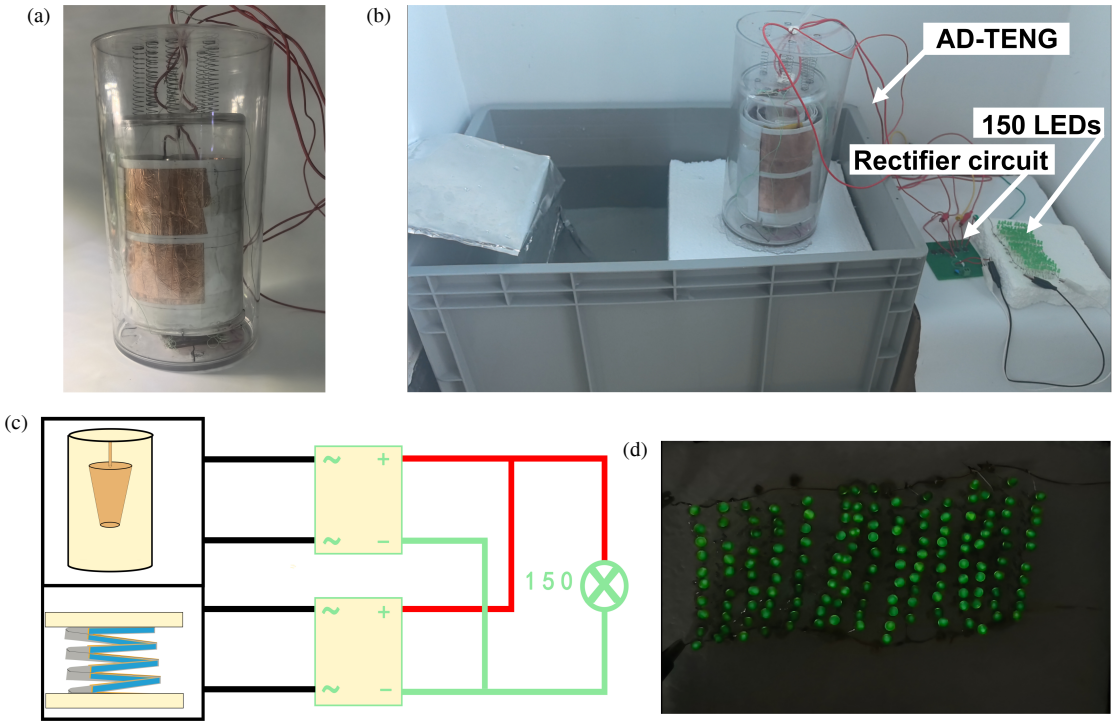

FIGURE 5. Applications of wave energy harvesting. (a) AD-TENG physical picture. (b) AD-TENG Water Working Diagram. (c) Diagram of the rectifier circuit with the small bulb lit up. (d) Small light bulb on the state image.

and 140 V. Fig. 3(i) mainly shows a simple schematic diagram of the overall motion simulation of AD-TENG being moved by waves. Fig. 3(j) clearly indicates that AD-TENG can harvest wave energy from all directions in the horizontal 360° and vertical directions. Through the experimental data, it can be seen that the superimposed output performance of SR-TENG and VF-TENG in the overall movement makes the overall output performance of AD-TENG higher, with Vpp reaching the maximum value of 162 V.

Figures 4(a) and (b) respectively show the trends of the output voltage and peak power of a single SR-TENG and VF-TENG with the change of the external load resistance. As shown in Fig. 4(a), under the condition of a frequency of 0.6 Hz, the voltage of SR-TENG increases with the increase of the load resistance, while the peak power initially increases and then decreases. When the matching resistance is set to 10 MΩ, the maximum peak power of SR-TENG is 0.5 mW. According to the test structure in Fig. 4(b), under the condition of a frequency of 0.6 Hz, the voltage output of VF-TENG increases with the increase of the load resistance, and the change in peak power is that it initially increases and then decreases with the increase of the load resistance. When the matching resistance is set to 10 MΩ, the maximum peak power of VF-TENG is 0.045 mW.

Then, as shown in Fig. 4(c), the SR-TENG and VF-TENG were connected in parallel using an integrated circuit board, and after rectification through a rectifier bridge, they were connected in parallel with capacitors of 10 μF, 22 μF, 100 μF, and 220 μF to test the charging time required to reach 3 V for different capacitance values. The test results are shown in Fig. 4(d). The 10 μF and 22 μF capacitance values reach 3 V within 1 minute; the 100 μF capacitance value reaches 3 V within 2 minutes; and the 220 μF capacitance value reaches 3 V within 6 minutes.

2.5. Applications of Wave Energy Harvesting

Finally, as shown in Fig. 5(a), the SR-TENG, VF-TENG, and spring were connected and encapsulated in an acrylic cylindrical bucket with a diameter of 15 cm and a height of 30 cm. To prevent corrosion by seawater, we carried out sealing treatment on the components. We filled the gaps with waterproof glue and used acrylic material, which is thick and less prone to cracking. It has certain resistance to general acid and alkali corrosion. At the same time, the internal material selects EVA foam with less light transmittance, which can block the direct sunlight. In addition, we conducted experiments on the peak voltage output of AD-TENG in a long-term environment with respect to the number of movements (in Fig. S2). From the images, it can be seen that as the number of movements increases, the output voltage changes little and remains relatively stable. This indicates that the device has good stability in long-term use. As can be seen in Fig. 5(b), the AD-TENG was applied in a simulated water wave oscillation environment. The overall structure of the AD-TENG has very few wirings. Due to the high structural integrity of the SR-TENG, compared with other TENG structures, each additional layer of electrode structure requires an additional wire. However, for the SR-TENG, the increase in the number of layers does not affect the number of wires, and only two wires, the negative and positive poles, are needed in total. As shown in Fig. 5(c), the SR-TENG and VF-TENG were connected in parallel using an integrated circuit board, and the

number of LED bulbs lit after rectification through a rectifier bridge was tested. As can be seen in Fig. 5(d), the AD-TENG successfully illuminates 150 LEDs.

3. CONCLUSIONS

In summary, we have designed and fabricated a bionic snail shell golden spiral TENG with excellent kinetic energy harvesting performance in both the horizontal and vertical directions.

- The innovative design uses a snail-inspired golden spiral structure for 360° horizontal energy harvesting.
- The system integrates the VF-TENG to achieve energy harvesting in vertical dimensions.
- The system charges a capacitor to 3 V within seconds and powers 150 LEDs.
- The highly integrated structure features simplified wiring.
- The curved friction layer with soft contact characteristics maximizes the effective contact area.
- The device achieves efficient energy collection from composite motions within tilt angle ranges.
- The system shows stable output ($\pm 4.6\%$ deviation) across 15 angles.

To further enhance the device's voltage regulation and energy buffering capabilities, our work will integrate a high-voltage power management solution specifically optimized for AD-TENG characteristics, employing a two-stage conversion topology (high-voltage rectification $\rightarrow$ intermediate DC bus $\rightarrow$ LDO regulation) to stabilize the pulsed output from 162 V to 3.3/5 V DC, while incorporating a hybrid energy storage system (supercapacitor + lithium-ion capacitor) with automatic switching via Schottky diodes to buffer intermittent power fluctuations [33]. Meanwhile, the AD-TENG's modular design and inherent omnidirectional adaptability make it highly suitable for scalable ocean energy harvesting networks. Here, we will provide an overview of the modular array deployment. The current compact design allows dense packing in floating arrays. Parallel interconnection of multiple AD-TENG units could linearly amplify power output (e.g., 100 units $\rightarrow\sim$ 50 mW at 0.6 Hz), while spatial distribution mitigates wave intermittency. Meanwhile, by integrating PMIC nodes based on a hierarchical step-down topology, synchronous power aggregation across array units is achieved (as previously mentioned). With further research and application. The AD-TENG shows great promise for marine applications through two primary implementations: (1) as self-powered sensors that can sustain long-term operation of IoT devices, such as buoys and salinity/temperature sensors, without relying on batteries — demonstrated by its ability to charge 220 µF capacitors within 6 minutes; and (2) as scalable arrays for blue energy grids, where its capacity to harvest multi-directional wave energy can support offshore platforms and help overcome the intermittency issues associated with traditional solar and wind energy systems.

4. EXPERIMENTAL SECTION

4.1. Fabrication of the AD-TENG

1. Cut a long strip of EVA substrate with a width of 12 cm and a thickness of 1 mm from the EVA foam board. Then, install copper electrodes with a thickness of 50 µm on both sides of the substrate and connect these electrodes with wires for output performance measurement. Additionally, cover the surface of the copper electrodes with a 50 µm FEP film and fix it firmly to the substrate. By installing a rotatable EVA foam board, the inner side of the EVA spiral layer adheres and is fixed to the outer wall of the pendulum. The pendulum is connected to a large acrylic cylindrical bucket through a non-elastic connecting rod, while the outer side of the EVA spiral layer adheres and is fixed to the inner wall of the acrylic cylindrical bucket with a diameter of 11 cm and a height of 20 cm. Meanwhile, the small acrylic cylindrical bucket is connected to the outer large acrylic cylindrical bucket through a spring.

2. A 5 cm wide and 56 cm long PET strip was cut from the PET plastic sheet as the base. copper electrodes with a thickness of 50 µm were installed on both sides of the base. Wires connected the electrodes to measure the output performance. A 50 µm thick FEP film was covered on the copper electrodes and fixed on the base. The upper and lower bases were respectively adhered and fixed to the inner and outer walls of two acrylic cylindrical barrels. The diameter of the large acrylic cylindrical barrel was 15 cm, and the height was 30 cm.

4.2. Electrical Measurement and Characterization

An experimental system was established to study the working characteristics of the proposed AD-TENG. A data acquisition system Keysight InfiniVision 2000 X from Keysight Technologies, Inc. was used to measure the electrical signals generated by the AD-TENG through the wires.

REFERENCES

[1] Zheng, H., Y. Zi, X. He, H. Guo, Y.-C. Lai, J. Wang, S. L. Zhang, C. Wu, G. Cheng, and Z. L. Wang, "Concurrent harvesting of ambient energy by hybrid nanogenerators for wearable self-powered systems and active remote sensing," *ACS Applied Materials & Interfaces*, Vol. 10, No. 17, 14 708–14 715, 2018.

[2] Yin, X., D. Liu, L. Zhou, X. Li, C. Zhang, P. Cheng, H. Guo, W. Song, J. Wang, and Z. L. Wang, "Structure and dimension effects on the performance of layered triboelectric nanogenerators in contact-separation mode," *ACS Nano*, Vol. 13, No. 1, 698–705, 2019.

[3] Yang, H., M. Deng, Q. Zeng, X. Zhang, J. Hu, Q. Tang, H. Yang, C. Hu, Y. Xi, and Z. L. Wang, "Polydirectional microvibration energy collection for self-powered multifunctional systems based on hybridized nanogenerators," *ACS Nano*, Vol. 14, No. 3, 3328–3336, 2020.

[4] Xia, K., J. Fu, and Z. Xu, "Multiple-frequency high-output triboelectric nanogenerator based on a water balloon for all-weather water wave energy harvesting," *Advanced Energy Materials*, Vol. 10, No. 28, 2000426, 2020.

[5] Xiang, H., L. Peng, Q. Yang, Z. L. Wang, and X. Cao, "Triboelectric nanogenerator for high-entropy energy, self-powered sensors, and popular education," *Science Advances*, Vol. 10, No. 48, eads2291, 2024.

[6] Saadatnia, Z., E. Esmailzadeh, and H. E. Naguib, "Design, simulation, and experimental characterization of a heaving triboelectric-electromagnetic wave energy harvester," *Nano Energy*, Vol. 50, 281–290, 2018.

[7] Baytekin, H. T., B. Baytekin, S. Soh, and B. A. Grzybowski, "Is water necessary for contact electrification?" *Angewandte Chemie-International Edition*, Vol. 50, No. 30, 6766–6770, 2011.

[8] Baytekin, H. T., A. Z. Patashinski, M. Branicki, B. Baytekin, S. Soh, and B. A. Grzybowski, "The mosaic of surface charge in contact electrification," *Science*, Vol. 333, No. 6040, 308–312, 2011.

[9] Wang, Z. L., "Triboelectric nanogenerators as new energy technology and self — Powered sensors-principles, problems and perspectives," *Faraday Discussions*, Vol. 176, 447–458, 2014.

[10] Cole, J. J., C. R. Barry, R. J. Knuesel, X. Wang, and H. O. Jacobs, "Nanocontact electrification: Patterned surface charges affecting adhesion, transfer, and printing," *Langmuir*, Vol. 27, No. 11, 7321–7329, 2011.

[11] McCarty, L. S. and G. M. Whitesides, "Electrostatic charging due to separation of ions at interfaces: Contact electrification of ionic electrets," *Angewandte Chemie International Edition*, Vol. 47, No. 12, 2188–2207, 2008.

[12] Yuan, F., S. Liu, J. Zhou, S. Wang, Y. Wang, S. Xuan, and X. Gong, "Smart touchless triboelectric nanogenerator towards safeguard and 3D morphological awareness," *Nano Energy*, Vol. 86, 106071, 2021.

[13] Xu, L., H. Wu, G. Yao, L. Chen, X. Yang, B. Chen, X. Huang, W. Zhong, X. Chen, Z. Yin, and Z. L. Wang, "Giant voltage enhancement via triboelectric charge supplement channel for self-powered electroadhesion," *ACS Nano*, Vol. 12, No. 10, 10 262–10 271, 2018.

[14] Xu, Y., W. Yang, X. Lu, Y. Yang, J. Li, J. Wen, T. Cheng, and Z. L. Wang, "Triboelectric nanogenerator for ocean wave graded energy harvesting and condition monitoring," *ACS Nano*, Vol. 15, No. 10, 16 368–16 375, 2021.

[15] Jiang, T., H. Pang, J. An, P. Lu, Y. Feng, X. Liang, W. Zhong, and Z. L. Wang, "Robust swing-structured triboelectric nanogenerator for efficient blue energy harvesting," *Advanced Energy Materials*, Vol. 10, No. 23, 2000064, 2020.

[16] Zhang, C., L. Zhou, P. Cheng, D. Liu, C. Zhang, X. Li, S. Li, J. Wang, and Z. L. Wang, "Bifilar-pendulum-assisted multilayer-structured triboelectric nanogenerators for wave energy harvesting," *Advanced Energy Materials*, Vol. 11, No. 12, 2003616, 2021.

[17] Xu, L., L. Xu, J. Luo, Y. Yan, B.-E. Jia, X. Yang, Y. Gao, and Z. L. Wang, "Hybrid all-in-one power source based on high-performance spherical triboelectric nanogenerators for harvesting environmental energy," *Advanced Energy Materials*, Vol. 10, No. 36, 2001669, 2020.

[18] Lin, Z., B. Zhang, Y. Xie, Z. Wu, J. Yang, and Z. L. Wang, "Elastic-connection and soft-contact triboelectric nanogenerator with superior durability and efficiency," *Advanced Functional Materials*, Vol. 31, No. 40, 2105237, 2021.

[19] Chen, A., C. Zhang, G. Zhu, and Z. L. Wang, "Polymer materials for high-performance triboelectric Nanogenerators," *Advanced Science*, Vol. 7, No. 14, 2000186, 2020.

[20] Dawson, N. M., P. M. Atencio, and K. J. Malloy, "Facile deposition of high quality ferroelectric poly (vinylidene fluoride) thin films by thermally modulated spin coating," *Journal of Polymer Science Part B: Polymer Physics*, Vol. 55, No. 3, 221–227, 2017.

[21] Wang, S., W. Tong, Y. Li, P. Zhang, Y. Liu, Y. Chen, and Y. Zhang, "Contributions of piezoelectricity and triboelectricity to a hydroxyapatite/PVDF–HFP fiber-film nanogenerator," *Nano Energy*, Vol. 105, 108026, 2023.

[22] Lin, Z., B. Zhang, H. Guo, Z. Wu, H. Zou, J. Yang, and Z. L. Wang, "Super-robust and frequency-multiplied triboelectric nanogenerator for efficient harvesting water and wind energy," *Nano Energy*, Vol. 64, 103908, 2019.

[23] Ding, M., J. Wang, D. Zhao, H. Li, X. Cheng, J. Wen, Z. L. Wang, and T. Cheng, "Magnetic-field-assisted triboelectric nanogenerator for harvesting multi-directional wave energy," *Nano Research*, Vol. 17, No. 8, 7144–7152, 2024.

[24] Wen, H., P. Yang, G. Liu, S. Xu, H. Yao, W. Li, H. Qu, J. Ding, J. Li, and L. Wan, "Flower-like triboelectric nanogenerator for blue energy harvesting with six degrees of freedom," *Nano Energy*, Vol. 93, 106796, 2022.

[25] Feng, Y., J. Han, M. Xu, X. Liang, T. Jiang, H. Li, and Z. L. Wang, "Blue energy for green hydrogen fuel: A self-powered electrochemical conversion system driven by triboelectric nanogenerators," *Advanced Energy Materials*, Vol. 12, No. 1, 2103143, 2022.

[26] Zhang, C., L. He, L. Zhou, O. Yang, W. Yuan, X. Wei, Y. Liu, L. Lu, J. Wang, and Z. L. Wang, "Active resonance triboelectric nanogenerator for harvesting omnidirectional water-wave energy," *Joule*, Vol. 5, No. 6, 1613–1623, 2021.

[27] Pang, H., Y. Feng, J. An, P. Chen, J. Han, T. Jiang, and Z. L. Wang, "Segmented swing-structured fur-based triboelectric nanogenerator for harvesting blue energy toward marine environmental applications," *Advanced Functional Materials*, Vol. 31, No. 47, 2106398, 2021.

[28] Sun, Y., F. Zheng, X. Wei, Y. Shi, R. Li, B. Wang, L. Wang, Z. Wu, and Z. L. Wang, "Pendular-translational hybrid nanogenerator harvesting water wave energy," *ACS Applied Materials & Interfaces*, Vol. 14, No. 13, 15 187–15 194, 2022.

[29] Xu, M., T. Zhao, C. Wang, S. L. Zhang, Z. Li, X. Pan, and Z. L. Wang, "High power density tower-like triboelectric nanogenerator for harvesting arbitrary directional water wave energy," *ACS Nano*, Vol. 13, No. 2, 1932–1939, 2019.

[30] Xiao, T. X., X. Liang, T. Jiang, L. Xu, J. J. Shao, J. H. Nie, Y. Bai, W. Zhong, and Z. L. Wang, "Spherical triboelectric nanogenerators based on spring-assisted multilayered structure for efficient water wave energy harvesting," *Advanced Functional Materials*, Vol. 28, No. 35, 1802634, 2018.

[31] Chen, Y., Y. Kuang, D. Shi, M. Hou, X. Chen, L. Jiang, J. Gao, L. Zhang, Y. He, and C.-P. Wong, "A triboelectric nanogenerator design for harvesting environmental mechanical energy from water mist," *Nano Energy*, Vol. 73, 104765, 2020.

[32] Jiang, W., H. Li, Z. Liu, Z. Li, J. Tian, B. Shi, Y. Zou, H. Ouyang, C. Zhao, L. Zhao, and e. al., "Fully bioabsorbable natural-materials-based triboelectric nanogenerators," *Advanced Materials*, Vol. 30, No. 32, 1801895, 2018.

[33] Moon, S.-Y., A. Shafique, S. C. Chandrarathna, and J.-W. Lee, "A high-voltage PMIC using an efficient perturb and observe technique for energy harvesting of triboelectric nanogenerators," *IEEE Transactions on Power Electronics*, Vol. 40, No. 2, 3225–3239, 2025.